The Crystal Structure of Cytochrome P460 of *Nitrosomonas europaea* Reveals a Novel Cytochrome Fold and Heme−Protein Cross-link[†,‡]

Arwen R. Pearson,[§,||] Bradley O. Elmore,[§] Cheng Yang,[⊥] Joseph D. Ferrara,[⊥] Alan B. Hooper,[§] and Carrie M. Wilmot*[,§]

Department of Biochemistry, Molecular Biology and Biophysics, The University of Minnesota, Minneapolis, Minnesota 55455, and Rigaku Americas Corporation, 9009 New Trails Drive, The Woodlands, Texas 77381

Received January 16, 2007; Revised Manuscript Received May 12, 2007

ABSTRACT: We have determined the 1.8 Å X-ray crystal structure of a monoheme *c*-type cytochrome, cytochrome P460, from *Nitrosomonas europea*. The chromophore possesses unusual spectral properties analogous to those of the catalytic heme P460 of hydroxylamine oxidoreductase (HAO), the only known heme in biology to withdraw electrons from an iron-coordinated substrate. The analysis reveals a homodimeric structure and elucidates a new *c*-type cytochrome fold that is predominantly β-sheet. In addition to the two cysteine thioether links to the porphyrin typical of *c*-type hemes, there is a third proteinaceous link involving a conserved lysine. The covalent bond is between the lysine side-chain nitrogen and the 13′-*meso* carbon of the heme, which, following cross-link formation, is sp^3-hybridized, demonstrating the loss of conjugation at this position within the porphyrin. The structure has implications for the analogous tyrosine−heme *meso* carbon cross-link observed in HAO.

The novel protein-bound *c*-type heme cofactor, heme P460, has to date been characterized in only two proteins, the enzyme hydroxylamine oxidoreductase (HAO)[1] and the small, soluble periplasmic cytochrome P460, both from the ammonia-oxidizing bacterium *Nitrosomonas europaea* or, in the case of cytochrome P460, also from the methylotroph *Methylococcus capsulatus* (*1*−*4*). Heme P460, named for its characteristic ferrous Soret peak maximum at 460 nm, has the distinction of being the only known heme in biology to withdraw electrons from an iron-coordinated substrate, as occurs during HAO turnover (*3*, *5*−*12*). HAO catalyzes the oxidation of hydroxylamine to nitrite, the second step in ammonia oxidation, a process that accounts for the majority of ammonia oxidation in the biosphere (*13*). HAO is a 210 kDa homotrimeric enzyme that, in addition to the three catalytic hemes P460, one from each subunit, contains 21 *c*-type hemes involved in electron transfer from the hemes P460 to their acceptor cytochromes (*14*, *15*). Cytochrome P460 is small by comparison, with a single high-spin, five-coordinate P460 heme per 18.8 kDa polypeptide, and bears no sequence similarity to HAO (*4*, *16*, *17*). The physiological function of cytochrome P460 has not been established, but it binds hydroxylamine, hydrazine, hydrogen peroxide, and cyanide in the ferric form and CO in the ferrous form and has a weak hydroxylamine oxidation/cytochrome *c* reduction activity (*2*, *5*, *17*−*19*). On the basis of sequence homology, secondary-structure prediction, and circular dichroism (CD) spectroscopy, cytochrome P460 is considered to be a member of a new family of small monoheme *c*-type cytochromes that are predominantly β-sheet (*20*, *21*).

The X-ray crystal structure of HAO to 2.8 Å resolution confirmed earlier biochemical studies showing that there was a protein-derived tyrosine cross-link to each catalytic heme P460, via a heme *meso* carbon, in addition to the two thioether bonds typical of *c*-type hemes (*6*, *15*). The crystal structure revealed that the tyrosine was from a neighboring subunit, effectively cross-linking the HAO trimer (*15*). Further, the planes of the tyrosine and heme ring were perpendicular, indicating that the heme *meso* carbon was sp^3-hybridized (*22*). Similar biochemical studies carried out on cytochrome P460 indicated that its heme P460 also possessed a third proteinaceous cross-link but, in this case, to a conserved lysine residue, K70 in *N. europea* (*23*, *24*). The presence of the third cross-link is responsible for the unusual electronic properties of heme P460, because cytochrome P460 in which K70 has been mutated to arginine or alanine has optical and ligand-binding properties typical of a *c*′-type heme (*24*). The formation of the cross-link to heme P460 in cytochrome P460 is probably an autocatalytic event; heterologous expression in *Pseudomonas aeruginosa* or *Escherichia coli* yields protein with identical spectral features to that of cytochrome P460 purified from source (*24*, *25*).

To compare the heme P460 structures in cytochrome P460 and HAO, and also to gain insight into the potential physiological function of cytochrome P460, we have recombinantly expressed, purified, and crystallized the cytochrome P460 of *N. europaea* (*25*). Here, we report the X-ray crystal structure determined to 1.8 Å resolution, which reveals a novel β-sheet-containing homodimeric cytochrome fold, as

[†] This work was funded by NIH GM-66569 (to C.M.W.), NSF MCB 0093447 (to A.B.H.), and DOE DE-FG02-95ER20191A009 (to A.B.H.).

[‡] Coordinates and structure factors have been deposited in the Protein Data Bank with accession codes 2je3 (cytochrome P460) and 2je2 (cytochrome P460 with additional hydroxyl on porphyrin).

* To whom correspondence should be addressed. Telephone: +1-612-624-2406. Fax: +1-612-624-5121. E-mail: wilmo004@umn.edu.

[§] The University of Minnesota.

[||] Present address: The Astbury Centre for Structural Molecular Biology, The University of Leeds, Leeds LS2 9JT, U.K.

[⊥] Rigaku Americas Corporation.

[1] Abbreviations: HAO, hydroxylamine oxidoreductase; CD, circular dichroism; PDB, Protein Data Bank.

10.1021/bi700086r CCC: $37.00
Published on Web 06/21/2007

Table 1: X-ray Data Collection Statistics[a]

	Cr K_α data	Cu K_α data (low X-ray dose; hydroxyl-modified)	Cu K_α data (high X-ray dose; native heme)
wavelength (Å)	2.29	1.54	1.54
temperature (K)	100	100	100
unit-cell parameters (Å, deg)	$a = b = 53.2$, $c = 127.0$, $\alpha = 90$, $\beta = 90$, $\gamma = 120$	$a = b = 53.3$, $c = 127.0$, $\alpha = 90$, $\beta = 90$, $\gamma = 120$	$a = b = 53.2$, $c = 127.0$, $\alpha = 90$, $\beta = 90$, $\gamma = 120$
space group	$P3_121$	$P3_121$	$P3_121$
rotation range (deg)	360	60	60
resolution (Å)	50−2.20 (2.28−2.20)	43−1.80 (1.86−1.80)	43−1.80 (1.86−1.80)
R_{merge} (%)[b]	3.9 (10.8)	4.3 (10.9)	3.9 (9.7)
completeness (%)	84.2 (11.5)	95.1 (72.3)	91.0 (57.2)
redundancy	18.6 (2.0)	4.4 (1.9)	3.6 (1.8)
$\langle I/\sigma(I)\rangle$	61.0 (12.2)	20.24 (3.8)	18.4 (3.8)
number of residues/asymmetric unit	178	178	178
number of anomalous scatterers/asymmetric unit	9 (5S, 1Fe, 3P)		
resolution range for phasing (Å)	15−2.8		
experimental $\langle\Delta F\rangle/\langle F\rangle$ (%) (phasing power)	1.57		
calculated $\langle\Delta F\rangle/\langle F\rangle$ (%) (for expected 5S and 1Fe)	2.88		
figure of merit[c] following phasing	0.854		

[a] Numbers in parentheses refer to the highest resolution shell. [b] $R_{merge} = \sum_{hkl}\sum_i|I_{hkl,i} - \langle I_{hkl}\rangle|/\sum_{hkl}\sum_i I_{hkl,i}$, where I is the observed intensity and $\langle I\rangle$ is the average intensity for multiple measurements. [c] Figure of merit $= \sqrt{x^2+y^2}$, where $x = (\sum_0^{2\pi}P(\alpha)\cos\alpha)/(\sum_0^{2\pi}P(\alpha))$, $y = (\sum_0^{2\pi}P(\alpha)\sin\alpha)/(\sum_0^{2\pi}P(\alpha))$, and the phase probability $P(\alpha) = \exp(A\cos\alpha + B\sin\alpha + C\cos(2\alpha) + D\sin(2\alpha))$, where A, B, C, and D are the Hendrickson−Lattman coefficients and α is the phase.

well as details of the lysine−porphyrin cross-link, whose nature differs unexpectedly from the equivalent cross-link in HAO.

MATERIALS AND METHODS

Structure Determination by Single-Wavelength Anomalous Diffraction at a Wavelength of 2.29 Å. The expression, purification, and crystallization of recombinant *Nitrosomonas europea* cytochrome P460 was carried out as previously described (*25*). A single crystal grown in 2.4 M sodium potassium phosphate at pH 5.0 was soaked for 1 min in artificial mother liquor containing 25% (w/v) xylitol before being flash-frozen in liquid nitrogen. X-ray diffraction data were collected using a MicroMax-007 Chromium source (wavelength of 2.29 Å) with VariMaxCr optics and a R-AXIS IV++ detector with a helium cone (Rigaku) (*26*). X-ray data collection was carried out at 100 K using an Xtreme-2000 (Rigaku).

Data were processed using HKL2000 (*27*). The CCP4 suite was used to calculate structure factors and anomalous differences from the measured intensities (*28*). Sulfur atoms in the protein scatter anomalously at a wavelength of 2.29 Å ($f'' = 1.14$ electrons), and this signal, along with the iron anomalous signal from the P460 heme ($f'' = 0.76$ electrons), was the basis for phasing the diffraction data by single-wavelength anomalous diffraction (SAD) methods. SHELXD was used to find initial anomalous peak positions (*29*). An iterative procedure of refinement and phase calculation using SHARP (*30*) followed by density modification and solvent flipping using DM and SOLOMON was used to resolve the phase ambiguity (*31*, *32*). Data processing and phasing statistics (Cr K_α data) are given in Table 1.

Model Building and Refinement. An initial model was built into the experimental density using COOT (*33*) and refined using REFMAC (*34*−*36*). Once the initial model was complete, phases were calculated and combined with amplitudes from a higher resolution dataset (1.8 Å resolution) collected using copper K_α radiation (wavelength of 1.54 Å) that has been previously described (*25*). Further cycles of model building and refinement were carried out using COOT and REFMAC (*34*−*36*) to yield a model with a R_{work} of 21.4% and a R_{free} of 25.6%. Because features were observed in the electron-density maps that suggested that X-ray-induced changes might have occurred at the heme during X-ray data collection, the 180° of copper K_α data were split, taking advantage of the high $P3_121$ symmetry, and the first and last 60° of data were processed independently using HKL2000 (*27*) as low and high X-ray dose datasets, respectively (Table 1). The CCP4 suite was then used to calculate structure factors for each dataset (*28*). Two models were thus refined: one using data from the beginning of data collection [low X-ray dose; Protein Data Bank (PDB) code 2je2] and the other using data from the end of data collection [high X-ray dose; PDB code 2je3] (Table 2). Cycles of building and refinement were performed using COOT (*33*) and REFMAC (*34*−*36*). The quality of the two structures was assessed using PROCHECK (*37*) and SFCHECK (*38*) (Table 2).

Investigation of X-radiation-Induced Changes. To investigate the X-ray-driven changes, datasets were collected for three further cytochrome P460 crystals, flash-frozen in liquid nitrogen (Methods in the Supporting Information), on beamline 4.2.2 at the Advanced Light Source (ALS), Berkeley, CA. X-ray diffraction data were collected at 1.239 Å and 100 K (Cryojet, Oxford Instruments) using the NOIR1 MBC detector. For each crystal, a different oscillation range per image was used but the exposure time per image was kept the same. This resulted in three datasets spanning the same total oscillation range (180°) but with different degrees of X-ray exposure. The first and last 60° of data for each crystal were processed independently with d*TREK, and the CCP4 suite used to calculate structure factors from the measured intensities (*28*, *39*). $2F_o - F_c$ and $F_o - F_c$ electron-density maps were then calculated using the high X-ray dose model (Table 2) and examined for positive features.

Table 2: X-ray Crystal Structure Refinement Statistics[a]

	low X-ray dose (hydroxyl-modified)	high X-ray dose (native heme)
resolution (Å)	43.4−1.8 (1.85−1.8)	43.4−1.8 (1.85−1.8)
completeness (%)	95.1 (72.3)	91.0 (56.1)
R_{work} (%)[b]	19.6 (28.3)	19.5 (29.6)
R_{free} (%)[b,c]	23.7 (34.5)	23.1 (30.5)
total number of reflections	17 631 (837)	17 344 (825)
number of reflections in the R_{work} set	16 679 (783)	16 423 (781)
number of reflections in the R_{free} set	952 (54)	921 (44)
number of non-hydrogen atoms	1430	1436
number of protein atoms	1258	1249
number of ligand atoms	59	58
number of solvent atoms	127	121
rmsd from ideality		
bonds (Å)	0.014	0.014
angles (deg)	1.641	1.655
average *B* factors		
main chain (Å^2)	26.0	26.6
side chain (Å^2)	27.1	27.7
ligands (Å^2)	25.0	27.8
solvent (Å^2)	36.6	38.5
Ramachandran plot		
allowed regions (%)	100	100
disallowed regions (%)	0	0
PDB codes	2je2	2je3

[a] Numbers in parentheses refer to the highest resolution shell. [b] *R* factor $= \sum||F_o| - |F_c||/\sum|F_o|$, where $|F_o|$ is the observed structure factor amplitude and $|F_c|$ is the calculated structure factor amplitude. [c] R_{free} is the *R* factor based on 5% of the data excluded from refinement.

Structural Analysis. Surface-area calculations were carried out using AREAIMOL (*40*). Internal cavities were identified in a dimer model of the refined high X-ray dose cytochrome P460 structure containing no waters using the CASTp server (*41*) and visualized using PyMOL (*42*). Possible exit channels from the internal cavities were assessed using the CAVER server (*43*) and again visualized using PyMOL (*42*). The out-of-plane distortions of the bound heme P460 from both cytochrome P460 and HAO were analyzed using the normal-coordinate structural decomposition method (*44*, *45*). Calculations of the out-of-plane and in-plane distortions of the porphyrin were carried out using the online normal-coordinate structure decomposition engine, version 3.0, at http://jasheln.unm.edu/jasheln/content/nsd/NSDengine/start.htm (*45*).

Mass Spectrometry. Samples of dissolved cytochrome P460 crystals and solutions of cytochrome P460 were desalted using Porus R2 resin (Applied Biosystems, Inc.). In brief, the samples were loaded onto the R2 resin and washed 5 times in 5% methanol and 3% formic acid. The samples were then eluted into a coated nanoelectrospray capillary (Protana Engineering) using 70% methanol and 3% formic acid. Electrospray mass spectra were acquired using a QSTAR Pulsar *i* quadrupole-TOF (time-of-flight) mass spectrometer equipped with a nano-ESI source (Protana Engineering). The ESI voltage was 1000 V; the TOF region acceleration voltage was 4 kV; and the injection pulse repetition rate was 6.0 kHz. External calibration was performed using human angiotensin II [monoisotopic mass (MH+) of 1046.5417; Sigma-Aldrich] and adrenocorticotropin hormone fragment 18−39 [monoisotopic mass (MH+) of 2465.1989; Sigma-Aldrich]. Mass spectra were the average of approximately 300 scans collected in the positive mode over a 5 min acquisition period.

Table 3: Mass Spectrometry of Cytochrome P460 Crystals

	theoretical mass (Da)[a]	observed mass (Da)[b]
CytP460	21 113.6	21 092.6 ± 0.4
CytP460 Δ32−39	20 270.7	20 269.2 ± 0.4
CytP460 Δ32−40 Δ82−84	19 904.3	19 885.2 ± 0.5

[a] Theoretical masses were calculated using ProtParam (*59*) and a mass of 616.5 Da for the bound heme. [b] Errors in the observed mass were calculated using the following equation: $\sqrt{(\sum(zE_z)^2 I_z)/(\sum I_z)} = 1/2E_{overall}$, where *z* is the charge species, E_z is the error in the measurement of charge species *z*, and I_z is the intensity of the charge species. E_z, *z*, and I_z are output by the deconvolution software for each peak used in the protein zero mass determination.

Sequence Alignment. Cytochrome P460 sequences were identified by a BLAST search against the *N. europaea* sequence and aligned using MAFFT (*46*, *47*).

RESULTS

Data collection and phasing statistics are shown in Table 1. A total of eight sites contributing to the measurable anomalous signal in the Cr K_α dataset (wavelength of 2.29 Å) were identified by SHARP, indicating the presence of two extra anomalous scatterers in addition to the five sulfurs and one iron known to be present in the cytochrome P460 monomer (Table 1). After phase improvement with SOLOMON and DM to 2.2 Å, the figure of merit was 0.854. The initial solvent-flattened map was extremely good, and 141 residues (total 178) were built manually using COOT (*33*). An anomalous difference electron-density map contoured at 4σ was used to guide building and revealed a ninth weak anomalous peak in addition to those identified by SHARP (Figure S1 in the Supporting Information). The three non-sulfur/non-iron anomalous peaks were assigned as bound phosphate ions, derived from the crystallization solution, on the basis of their anomalous signal, $2F_o - F_c$ density, and surrounding environment. Phosphorus has a greater anomalous signal than iron ($f''_P = 0.91$, $f''_{Fe} = 0.76$, and $f''_S = 1.14$) at 2.29 Å; however, the anomalous difference density for two of the bound phosphates was weaker than that of the iron and presumably reflects a lower occupancy. Clear density for the heme was visible in the solvent-flattened map (Figure S2 in the Supporting Information), and idealized coordinates for a *c*-type heme obtained from the HIC-UP server (*48*) were inserted using the *find ligands* feature of COOT. The initial model was refined using REFMAC to a R_{work} of 25.6% ($R_{free} = 31.0\%$) (*34*−*36*).

This initial model was then combined with the 1.8 Å native dataset, and iterative cycles of refinement and model building were carried out to yield a model containing 156 residues, a *c*-type heme, and three bound phosphate ions (Figure S1 in the Supporting Information). The C-terminal lysine and the C-terminal six-histidine tag are not visible in the electron density. In addition, there are two breaks in the electron density encompassing residues 31−40 and 82−84. Mass spectrometry of dissolved crystals revealed at least three species in significant amounts (Table 3), confirming that proteolysis had occurred during crystallization. The first species corresponded well to the protein lacking residues 32−39, suggesting that residues 31 and 40 are present but

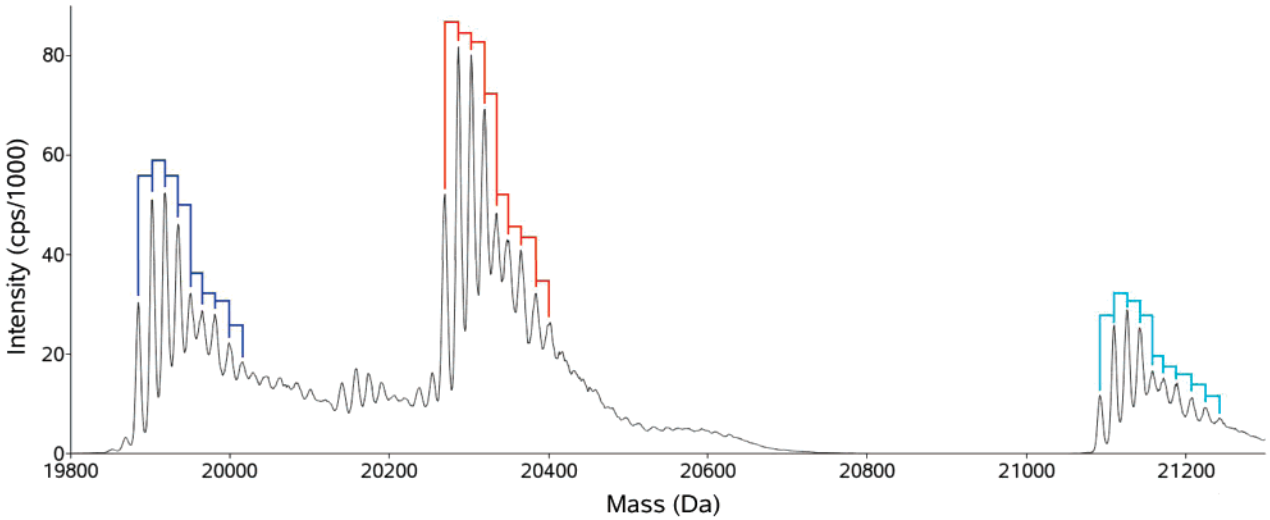

FIGURE 1: Deconvoluted mass spectrum of dissolved cytochrome P460 crystals reveals extensive oxidation and proteolysis. The cyan peaks correspond to the full-length cytochrome P460; the red peaks correspond to cytochrome P460 Δ32−39; and the dark blue peaks correspond to cytochrome P460 Δ32−40 Δ82−84. The peak steps best fit to successive oxidations.

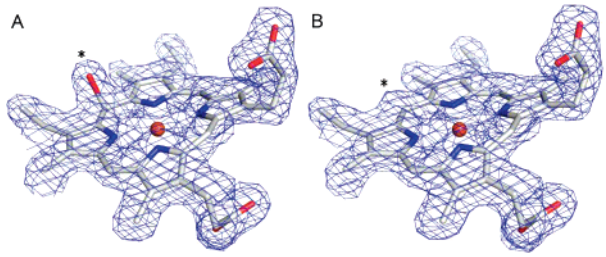

FIGURE 2: (A) $2F_o - F_c$ density contoured at 1σ, calculated from the first 60° of X-ray exposure. Heme P460 is shown in sticks colored by the element, and the bound hydroxyl is also modeled. (B) Same view showing $2F_o - F_c$ density contoured at 1σ, calculated from the third 60° of X-ray exposure. In both views, an asterisk marks the position of the bound hydroxyl. The figure was generated using PyMOL (*42*).

disordered in the electron-density map. The second species corresponded best to the protein lacking residues 32−40 and 82−84. The third species corresponded best to full-length cytochrome P460. The mass spectrometry also revealed that extensive oxidation was occurring in all three species, with oxidation trains corresponding to the addition of up to eight extra oxygens (Figure 1); however, only one additional oxygen atom was unequivocally observed in the electron-density map. Maps calculated using the full 1.8 Å resolution native dataset revealed extra density off the 5′-*meso* carbon of the porphyrin, which is on the solvent-exposed side of the heme. This density was modeled initially as a water, but after refinement, the C−O distance was 1.9 Å, indicating that the feature was most likely a covalently bound hydroxyl. To determine whether this oxidation had occurred during X-ray data collection, the first and last 60° of the 180° X-ray diffraction data were processed independently (low and high X-ray dose respectively, Table 1) and electron-density maps were calculated. Surprisingly, the hydroxyl was only present in the first 60° of data and not in the final 60° and therefore, presumably, has been lost through reduction of the oxidized porphyrin by X-ray-derived photoelectrons (Figure 2). To confirm that this was not an artifact, we collected X-ray diffraction data on three other cytochrome P460 crystals (Table S1 in the Supporting Information). Examination of maps calculated using the first and last 60° of each of these crystals gave the same result as observed for the 1.8 Å in-house X-ray dataset, confirming that the hydroxyl was only present at the start of data collection. In addition, these data showed that, with longer exposure over the same oscillation range, the hydroxyl occupancy decreased proportionately to the X-ray dose (Figure S3 in the Supporting Information). Crystal structures for both the first (low X-ray dose, hereafter referred to as "hydroxyl-modified", PDB code 2je2) and last (high X-ray dose, hereafter referred to as "native heme", PDB code 2je3) 60° of the in-house data were therefore refined independently (Table 2) and showed that there was no difference in the overall structure [root-mean-square deviation $(\text{rmsd})_{XYZ} = 0.28$ Å, and $\text{rmsd}_B = 3.09$ Å^2]. $F_o - F_o$ maps indicated that all structural changes occurring during radiation exposure were localized to the heme and reflected the loss of the bound hydroxyl and slight movements in the position of the iron relative to the heme (Figure S4 in the Supporting Information).

Both final models reveal a novel *c*-type heme-binding fold that consists of a twisted five-stranded antiparallel β sheet (B2−B6) flanked by three large helices (H2, H4, and H6), three helical turns (H1, H3, and H5), and a second, short two-strand β hairpin (B1 and B7) (Figures 3 and 4 and Figure S1 in the Supporting Information). The overall monomer structure is L-shaped, with the β sheet forming the back of the L and the heme-binding helix (H4) forming the base of the L. A search of the DALI server indicates that this fold has no structural homology to any other heme-binding protein and therefore represents a new class of type II β-sheet *c*-type cytochromes (*49*). The structure does have weak structural homology ($z < 5$) to several proteins; however, in all cases, this is restricted to the five-stranded β sheet (Table S2 in the Supporting Information).

Although only a monomer is present in the asymmetric unit, cytochrome P460 is clearly dimeric, with an extensive dimer interface formed along the crystallographic 2-fold axis, burying 21% of the surface of each monomer. In addition, two β strands (B4 and B5) are extended out of the sheet and reach around to the heme-binding pocket of the other monomer (Figure 4). However, the residues at the tip of this

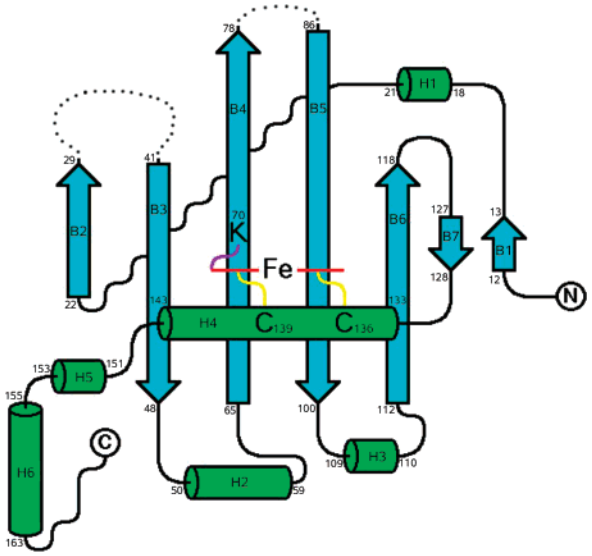

FIGURE 3: Schematic representation of cytochrome P460 topology showing β sheets as cyan arrows and α helices as green rods. Missing residues are indicated by dotted lines. In addition, the relative position of the heme P460 and its three covalent cross-links (Cys−heme in yellow and Lys−heme in purple) are shown. The figure was generated using TopDraw (*60*).

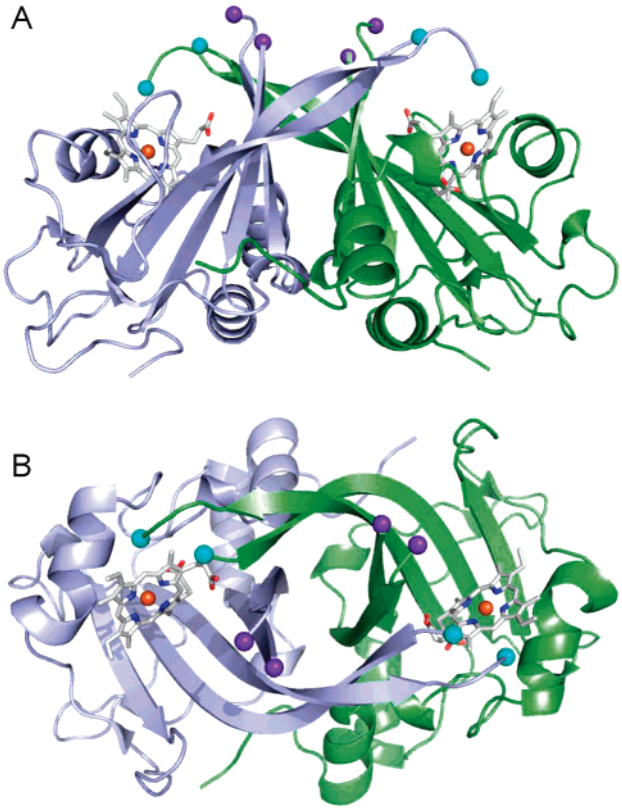

FIGURE 4: (A) Cytochrome P460 crystallographic dimer displayed as a secondary-structure cartoon. Monomer A is colored green, and monomer B is colored purple. Heme P460 is shown as sticks colored by the element, with the iron shown as an orange sphere. Breaks in the polypeptide chain are indicated by sphere pairs (break 31−40, purple spheres; and break 82−84, cyan spheres). (B) Same image rotated 90° around its horizontal axis. The figure was generated using PyMOL (*42*).

arm, G82, S83, and G84, are not visible in the electron density.

Sequence alignment of 29 cytochrome P460 primary sequences indicates 6 absolutely conserved residues, including the heme-binding residues K70, C136, C139, and H140 (Figure S5 in the Supporting Information). Most of these cluster at the base of the cytochrome P460 monomer, where the identical residues D147 (between H4 and H5) and W112 (B6) form a hydrogen-bonding network with the highly conserved residue K100 (B5) and the semiconserved residue D64 (B4) that zips up the base of the β sheet and also stabilizes the heme-binding helix H4. There are additionally two adjacent internal cavities lined by residues that show some conservation (Figure 5A and Figure S6 in the Supporting Information). The cavity on the proximal side of the heme (red mesh in Figure 5) has a volume of 32.5 Å^3 and is lined by the conserved residues W112, an aromatic residue (F114 in *N. europea*), the semiconserved V149, the nonconserved residue S98, and the backbone carbonyl of M148. It contains a buried water molecule (blue sphere in Figure 5) coordinated by S98 and the O1A propionate oxygen of the heme. This cavity is linked by a narrow channel (minimum radius of 1 Å), formed by the semiconserved V149, the nonconserved T68, and the aliphatic portion of the same heme propionate group, to a second more hydrophobic cavity (blue mesh in Figure 5A) lined by the semiconserved F62 and V149 (common to both cavities), the weakly conserved residue V24, and the nonconserved residues V46, V48, T68, and Y154. This cavity is empty, although it is large enough (23.3 Å^3) to contain a small diatomic, such as O_2 (volume of 18.2 Å^3) (*50*). Although the cavity that lies proximally beneath the heme is close to

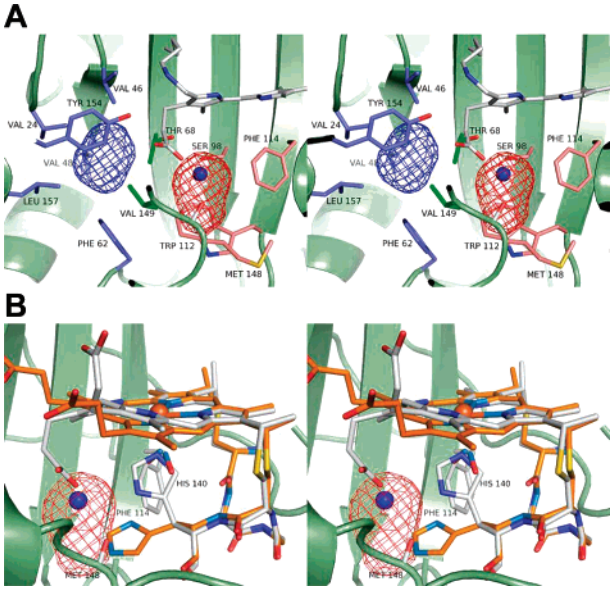

FIGURE 5: (A) Stereo image of the internal cavities in cytochrome P460. Cytochrome P460 is shown as a green secondary-structure cartoon. The cavities are represented by red and blue mesh nets. The heme P460 and cavity-lining residues are drawn as sticks and colored by the element, but with differential carbon coloring (gray, heme P460; pink, associated with the red cavity only; blue, associated with the blue cavity only; and green, between the two cavities). The ordered water located in the red cavity is shown as a blue sphere. (B) Stereo overlay of cytochrome P460 with reduced *A. xylosoxidans* cytochrome *c′* in complex with NO (PDB code 1e85) (*55*). Cytochrome P460 and the cavity are represented the same as in A, except all carbon atoms are gray. The *A. xylosoxidans* cytochrome *c′* heme, proximal His, and two NO conformers are drawn as sticks and colored by the element, with carbon atoms colored orange. Cavities were identified using the CASTp server (*41*). The figures were generated using PyMOL (*42*).

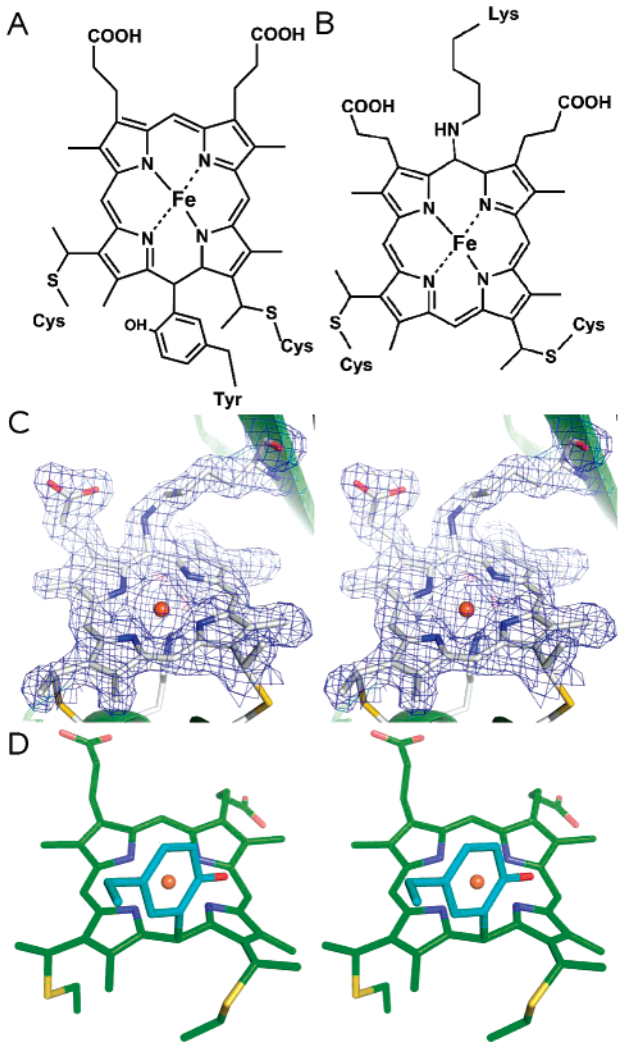

FIGURE 6: (A) Schematic of the heme P460 structure in HAO. (B) Schematic of the heme P460 structure in cytochrome P460. (C) Stereo image of the experimentally observed structure of heme P460 in cytochrome P460. Native heme $2F_o - F_c$ density contoured at 1σ is shown as a blue mesh; heme P460, K70, C136, C139, and H140 are shown as sticks colored by the element; and the protein is shown as a green secondary-structure cartoon. (D) Stereo image of the X-ray crystal structure of heme P460 in HAO, derived from subunit B of PDB code 1fgj (*15*). Heme P460 is shown as sticks colored by the element. The tyrosine is cyan. The tyrosine comes from a neighboring subunit. The figure was generated using PyMOL (*42*). Heme P460 in C and D are shown in the same relative orientation.

the surface of the molecule, neither cavity has clear access to the external solvent. Exit channel calculations indicate choke points for both cavities (channel radii of 0.72 and 0.82 Å, respectively).

The heme group sits on the shelf-like base of the monomer and, as expected, is covalently bound to the protein via the two cysteines of the *c*-type heme-binding motif, C136 and C139, with the proximal ligand to the heme being H140. In addition, there is a third covalent linkage to the porphyrin ring from the absolutely conserved residue K70 clearly present in both the hydroxyl-modified and native heme structures, as was predicted by biochemical studies (*23*, *24*). As in the heme P460 of HAO, the third cross-link is to a *meso* carbon of the porphyrin ring. However, in cytochrome P460, the cross-link is to the 13′-*meso* carbon, opposite the 5′-*meso* carbon linked to tyrosine in HAO (parts A and B of Figure 6). K70 of cytochrome P460 is cross-linked to the porphyrin ring via its side-chain nitrogen, and it is clear from the structure that this linkage results in an sp^3 carbon at the 13′-*meso* carbon of the porphyrin (Figure 6C).

A phosphate ion originating from the crystallization mother liquor is bound to the distal side of the heme (Figure 7). The low relative peak height for the bound phosphate with respect to the iron in the anomalous difference electron-density map suggests that the phosphate site is only partially occupied, and this is confirmed by its increased B values with respect to the surrounding atoms (~2-fold greater). The phosphate is coordinated by the nonconserved residue E96, which sits at one side of the putative distal ligand-binding pocket above the heme. Two other bound phosphates are present (Figure S1 in the Supporting Information). The first is strongly bound in a surface pocket by the semiconserved residue T151 and the nonconserved residues R158 and K145 and is also ligated by two waters. The second phosphate is much less strongly bound, as is reflected by a low peak height in the anomalous difference map, and is bound at a crystal contact with a crystallographically related monomer from another dimer.

The heme moiety of cytochrome P460 is extremely buckled. Analysis using normal-coordinate structure decomposition (*44*, *45*) revealed that the heme conformation can be decomposed into almost equal contributions from *saddled* and *ruffled* deformations with little difference caused by the presence of the hydroxyl on the 5′-*meso* carbon (hydroxyl-modified structure: *sad*, −0.7 Å; *ruf*, −0.7 Å and native heme structure: *sad*, −0.8 Å; *ruf*, −0.7 Å), with a secondary contribution from a waving deformation in both the hydroxyl-modified and native heme structures [*wav*(*x*) 0.5 Å]. Analyses of numerous cytochrome structures have suggested that the out-of-plane distortions of protein-bound heme groups reflect their function and catalytic activity (*44*). Therefore, the same analysis was carried out on the two crystallographically independent hemes P460 of HAO (*15*). Both of these hemes show a strong contribution from the ruffled deformation (*ruf* = −1.4 and −1.5 Å), with minor contributions from other deformation modes (*sad*, *dom*, *wav*(*x*) = ±0.3−0.4 Å).

DISCUSSION

The X-ray crystal structure reported here reveals a new *c*-type heme-binding fold that is predominantly β-sheet with flanking helices. This is the first structural characterization of a member of a new family of *c*-type cytochromes that had been predicted on the basis of secondary-structure prediction and CD spectra to be mainly β-sheet. This family consists of two subfamilies: cytochromes P460 and cytochromes *c*′-beta (*20*, *21*).

Although HAO and cytochrome P460 both contain heme P460, the only similarity in fold is the *c*-type heme-binding helix containing the CXXCH motif. In addition, the location of the extra cross-link to the opposite sides of the porphyrin ring indicates that the unusual spectral properties of heme P460 do not require the cross-link to be with a specific *meso* carbon of the heme. This observation demonstrates that the formation of heme P460 can occur in multiple protein scaffolds, although it has thus far only been identified in these two proteins.

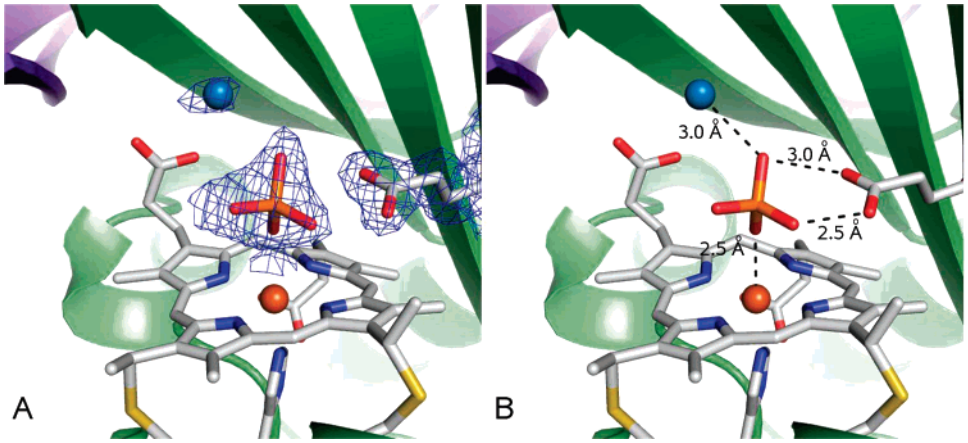

FIGURE 7: (A) $2F_o - F_c$ electron density contoured at 1σ, showing the heme P460 distally bound phosphate ion. Also shown is E96 and a water (blue sphere), which also coordinate the phosphate. Heme P460, C136, C139, H140, E96, and phosphate are shown as sticks colored by the element, and the protein is shown as a green (monomer A) and purple (monomer B) secondary-structure cartoon. The cross-linked K70 is omitted for clarity. (B) Same view showing the interactions made by the phosphate. The figure was generated using PyMOL (*42*).

The excellent quality of the electron-density map makes it clear that the formation of the lysine−heme cross-link results in the 13′-*meso* carbon of the heme adopting a tetrahedral geometry, suggesting that the carbon is now sp^3 instead of sp^2, and confirming similar observations made using the 2.8 Å crystal structure of HAO (parts C and D of Figure 6) (*15*, *22*). This disruption of electron delocalization around the heme is likely responsible for the unusual spectral properties, including the Mössbauer and Raman spectra of heme P460 (*18*). The formation of the lysine−heme cross-link, which appears to be autocatalytic because the cofactor still forms even when cytochrome P460 is expressed heterologously, can be envisaged to occur via a nucleophilic attack by the lysine amino group lone pair at the *meso* carbon of the heme, in much the same way as the proposed mechanism of formation of lysine tyrosylquinone, the protein-derived cofactor of lysyl oxidase (*51*). Alternatively, a radical mechanism, common in heme modification, may be responsible (*52*). Nuclear magnetic resonance (NMR) analysis of fragments of HAO produced by enzymic proteolysis revealed only three tyrosine aromatic ring proton resonances (*6*). On this basis, the tyrosine cross-link in HAO has been reported to be from a ring carbon of the tyrosine to the heme (*6*, *15*). Unfortunately, the crystal structure of HAO was not at sufficiently high resolution to unambiguously assign the nature of the tyrosine−heme cross-link, and the final structure, in which the Cϵ1 carbon of tyrosine is linked to the heme, appears to have relied heavily on the proposed structure from the previous NMR studies (*6*, *15*). However, forcing the C−C linkage results in an unlikely position for the tyrosine hydroxyl group, which is sterically clashing with a porphyrin carbon (1.5 and 2.1 Å in the two crystallographically independent HAO monomers). Mass spectrometry of proteolyzed fragments of HAO demonstrated that only one covalent bond was present between the tyrosine and the porphyrin (*6*). We suggest, on the basis of the heme P460 structure reported here, that the tyrosine−heme cross-link in HAO is more likely to be between the tyrosine oxygen and the heme and to form by a similar process as the lysine−heme cross-link of cytochrome P460.

Mass spectrometry of freshly purified cytochrome P460 shows a single peak at the expected mass (*25*). However, mass spectrometry of the dissolved crystals shows that, as well as proteolysis, there is evidence of extensive oxidation (Figure 1). This is even more pronounced in older protein that has been stored in solution at 4 °C, which shows extensive proteolysis, as well as extensive oxidation trains when examined by mass spectrometry (data not shown). These observations suggest that the heme-bound hydroxyl observed in the cytochrome P460 hydroxyl-modified structure is nonphysiological (PDB code 2je2) and that the native heme structure (PDB code 2je3) is more representative of the true physiological structure of cytochrome P460. The hydroxyl-modified structure is unusual in that the hydroxyl-bearing 5′-*meso* carbon of the porphyrin is also sp^3-hybridized (Figure 2). To our knowledge, this is the first example of a stable porphyrin derivative with two trans *meso* sp^3 carbons.

The susceptibility of the 5′-*meso* carbon position in cytochrome P460 to oxidation, as evidenced here by the electron density and mass spectrometry, demonstrates the reactivity of the porphyrin *meso* position opposite the lysine site to nucleophilic attack. Interestingly, the treatment of ferric HAO with excess hydrogen peroxide resulted in the loss of both catalytic activity and the 460 nm spectral feature associated with heme P460, although none of the remaining classical *c*-type hemes were affected (*11*). This may reflect a similar sensitivity to oxidation of the heme P460 in both HAO and cytochrome P460. The "opposite" *meso* carbon of mature heme P460 apparently derives its reactivity from alterations in the heme properties induced by the hybridization of the cross-linked *meso* carbon to sp^3 during the formation of the cross-link with lysine or tyrosine. Further studies are underway to determine whether the reactivity of this "opposite" *meso* carbon of mature hemes P460 might have a biological role.

The present structure clearly indicates that cytochrome P460 is an obligate dimer and resolves the ambiguity in previous reported studies, which suggested that cytochrome P460 was either di- or trimeric (*2*, *17*, *19*). The present structure also reveals a surprisingly exposed pentacoordinate heme P460; nearly the entire top face of the heme is exposed to the solvent. This cleft is presumably involved in ligand binding and function. E96, which hydrogen bonds to the

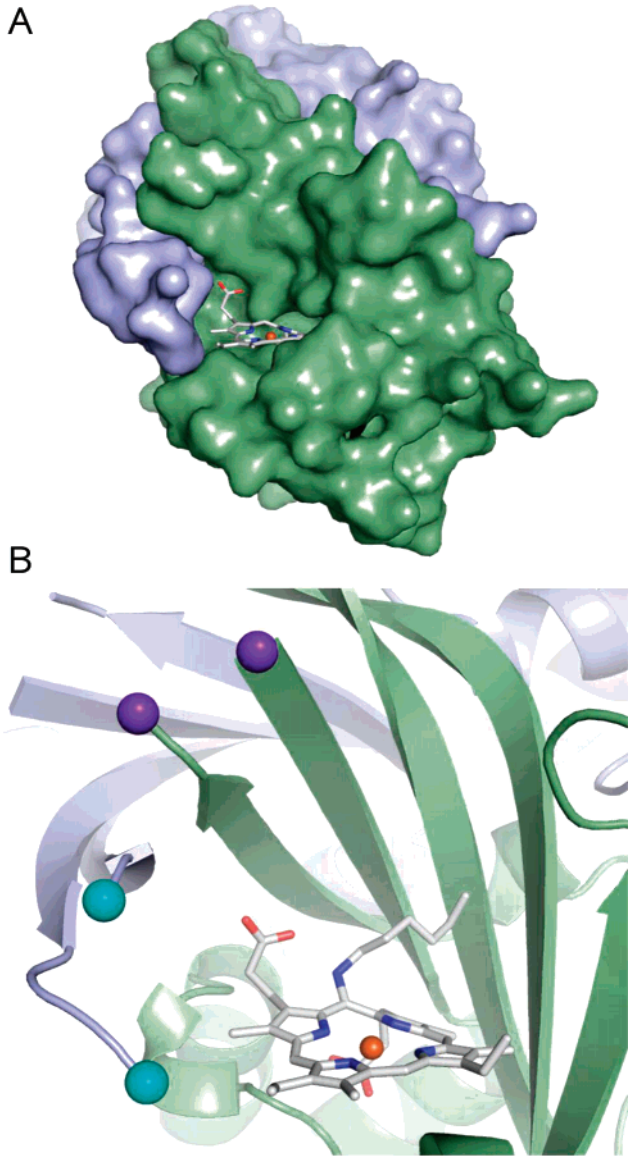

FIGURE 8: (A) Surface representation of the cytochrome P460 dimer showing the heme P460 binding cleft. Monomer A is colored green, and monomer B is colored purple. (B) Location of the missing loop 31−40 in relation to heme P460 in the same orientation as in A. Monomer A is shown as a green secondary-structure cartoon, and monomer B is shown as a purple cartoon. Purple balls indicate the start and finish of the missing loop 31−40, and cyan balls indicate the start and finish of the missing loop 82−84 from monomer B. Heme P460 and K70 are shown as sticks colored by the element. The figure was generated using PyMOL (*42*).

phosphate ion bound to the distal side of the heme, could be involved in the binding of small ligands, such as hydroxylamine, hydrazine, CO, hydrogen peroxide, and cyanide, known to interact with *N. europea* cytochrome P460 (Figure 7) (*2*, *17*, *19*). Although not conserved, it has an interesting pattern of variation (E, Q, D, T, and F), where the range in amino acid size and properties may confer heme distal ligand-binding specificity (Figure S5 in the Supporting Information). The β arm that reaches around from the other monomer to the heme site partially occludes the heme. However, even when the three disordered or missing residues at the tip of the loop (82−GSG−84) are taken into account, the heme is still very accessible (Figure 8A). A second region of 10 residues (*31*−*40*) is not visible in the electron-density map, and mass spectrometry of dissolved crystals suggests at least 8 of these residues have been lost through proteolysis. Residues 30 and 41 form the tips of two antiparallel β strands that are positioned just above the heme (Cα of P30 is 17.1 Å away from the iron, and Cα of T41 is 17.4 Å away) (Figure 8B). It is possible that this missing loop could fold down over the heme and help shield it from the solvent as well as coordinate bound ligands. Interestingly, this loop is extremely divergent in predicted cytochromes P460, both in sequence and in length (4−22 residues), suggesting that this loop may play a role in ligand or partner protein binding and specificity (Figure S5 in the Supporting Information). Future studies may also reveal whether the heme is at least partially shielded by a protein partner that was lost during purification. Cytochrome P460 of *M. capsulatus*, for example, copurifies with a cytochrome *c*′ (*4*).

It is not clear at this time if cytochromes P460 share a common function or have different functions in different organisms. The distal heme ligand-binding site, here occupied by a phosphate ion (Figure 7), has considerable variability in the amino acid identities surrounding this position and thus may have different distal ligand-binding properties and physiological functions. In addition, the variable length of the structurally missing loop in different cytochromes P460 may lead to very different solvent-exposure patterns on the distal side of the heme. The limited available *in vitro* data may also be in keeping with differences in physiological function (*4*, *17*). The *M. capsulatus* cytochrome P460 has equivalent hydroxylamine oxidation activity to the HAO from *N. europea* and therefore has been suggested to function *in vivo* as a hydroxylamine oxidoreductase (*53*). In contrast, the preparation of *N. europea* cytochrome P460, whose structure is presented in this study, has weak hydroxylamine oxidation activity compared to *N. europea* HAO (*17*).

Cytochrome P460 is sequentially related to a new structural class of high spin cytochromes *c*′ that are predominantly β-sheet (*21*) yet has some ligand-binding properties in common with the 4-helix bundle cytochromes *c*′ found in denitrifying bacteria (*54*, *55*). These cytochromes *c*′ have been proposed to mediate the transfer of nitric oxide and/or to protect the organism from NO toxicity (*56*). The crystal structure of reduced *Alicaligenes xylosoxidans* cytochrome *c*′ in complex with NO revealed a highly unusual mode of binding in which the proximal His ligand of the five-coordinate iron was replaced by NO to give a five-coordinate NO−heme complex (*54*, *55*). Time-resolved resonance Raman and absorption studies, coupled with molecular dynamics simulations in this system, indicated that NO first binds distally to the heme in a six-coordinate complex (*57*). The proximal His ligand to the iron dissociates because of trans effects and is replaced by another NO to form a transient bisnitrosyl six-coordinate species prior to dissociation of the distal NO to yield the final five-coordinate species (Figure 5B). Interestingly, there is also a proximal cavity in this cytochrome *c*′, which is large enough to hold a diatomic gas. When CO binds distally to form a six-coordinate complex with this cytochrome *c*′, a second molecule of CO is bound in a cavity on the proximal side of the heme adjacent to the proximal His ligand to the iron (*54*). Thus, the presence of two cavities in cytochrome P460 adjacent to the proximal His ligand to the heme P460 may have physiological significance (Figure 5A and Figure S6 in the

Supporting Information). Finally, as noted previously (*21*), putative cytochrome P460 sequences are found in a number of pathogenic species, such as *Burkholdaria cenocepacia*, an opportunistic pathogen of cystic fibrosis sufferers (EAM21795, Figure S5 in the Supporting Information) (*58*). Thus, cytochrome P460 may play a role in the NO defense of these organisms against macrophages and neutrophils and could represent a possible drug target. Indeed, NO binds to cytochrome P460 very effectively (Arciero, Elmore, and Hooper, unpublished results).

In summary, the structure of cytochrome P460 represents the first structurally characterized member of a new class of dimeric β-sheet *c*-type cytochromes. Further studies are underway with both cytochrome P460 and HAO to correlate the properties of cross-linked hemes P460 to their biological function.

ACKNOWLEDGMENT

This work was carried out using computer resources in the Basic Sciences Computing Laboratory of the University of Minnesota Supercomputing Institute, and we thank Patton Fast and Benjamin Lynch for their support. Mass spectrometry studies were carried out at the Center for Mass Spectrometry and Proteomics at The University of Minnesota, and we thank Sudha Marimanikkuppam for assistance. X-ray data were collected at the Kahlert Structural Biology Laboratory (KSBL) at The University of Minnesota (supported by a Minnesota Partnership for Biotechnology and Medical Genomics Grant SPAP-05-0013-P-FY06), Rigaku Americas Corporation, TX, and beam-line 4.2.2 at the Advanced Light Source (ALS), Lawrence Berkeley National Laboratory (LBNL), Berkeley, CA. The Advanced Light Source is supported by the Director, Office of Science, Office of Basic Energy Sciences of the U.S. Department of Energy under contract number DE-AC02-05CH11231. We thank Ed Hoeffner for KSBL support and Jay Nix, Kelsey Newell, and Elena Kovaleva for help with ALS data collection.

SUPPORTING INFORMATION AVAILABLE

Crystal growth, freezing conditions, and X-ray data collection method for X-ray diffraction data collected at beamline 4.2.2, ALS; Table S1, X-ray data collection statistics for data collected at beamline 4.2.2, ALS; Table S2, results of the structural homology search using the DALI server, showing all hits with $z > 2.5$; Figure S1, anomalous difference electron density; Figure S2, quality of initial phased electron density at the heme; Figure S3, X-ray-derived changes are X-ray-dose-dependent; Figure S4, X-ray-derived changes are localized to the heme moiety; Figure S5, alignment of 29 predicted cytochrome P460 sequences; Figure S6, two internal cavities are located on the proximal side of the heme. This material is available free of charge via the Internet at http://pubs.acs.org.

REFERENCES

1. Bergmann, D. J., Zahn, J. A., Hooper, A. B., and DiSpirito, A. A. (1998) Cytochrome P460 genes from the methanotroph *Methylococcus capsulatus* Bath, *J. Bacteriol. 180*, 6440−6445.
2. Erickson, R. H., and Hooper, A. B. (1972) Preliminary characterization of a variant co-binding heme protein from *Nitrosomonas*, *Biochim. Biophys. Acta 275*, 231−244.
3. Hooper, A. B., Maxwell, P. C., and Terry, K. R. (1978) Hydroxylamine oxidoreductase from *Nitrosomonas*—Absorption spectra and content of heme and metal, *Biochemistry 17*, 2984−2989.
4. Zahn, J., Duncan, C., and DiSpirito, A. A. (1994) Oxidation of hydroxylamine by cytochrome P460 of the obligate methylotroph *Methylococcus capsulatus* Bath, *J. Bacteriol. 176*, 5879−5887.
5. Andersson, K. K., Kent, T. A., Lipscomb, J. D., Hooper, A. B., and Munck, E. (1984) Mössbauer, electron paramagnetic resonance, and optical studies of the P460 center of hydroxylamine oxidoreductase from *Nitrosomonas*—A ferrous heme with an unusually large quadrupole splitting, *J. Biol. Chem. 259*, 6833−6840.
6. Arciero, D. M., Hooper, A. B., Cai, M., and Timkovich, R. (1993) Evidence for the structure of the active-site heme-P460 in hydroxylamine oxidoreductase of *Nitrosomonas*, *Biochemistry 32*, 9370−9378.
7. Hendrich, M. P., Logan, M., Andersson, K. K., Arciero, D. M., Lipscomb, J. D., and Hooper, A. B. (1994) The active-site of hydroxylamine oxidoreductase from *Nitrosomonas*—Evidence for a new metal cluster in enzymes, *J. Am. Chem. Soc. 116*, 11961−11968.
8. Hendrich, M. P., Petasis, D., Arciero, D. M., and Hooper, A. B. (2001) Correlations of structure and electronic properties from EPR spectroscopy of hydroxylamine oxidoreductase, *J. Am. Chem. Soc. 123*, 2997−3005.
9. Hendrich, M. P., Upadhyay, A. K., Riga, J., Arciero, D. M., and Hooper, A. B. (2002) Spectroscopic characterization of the NO adduct of hydroxylamine oxidoreductase, *Biochemistry 41*, 4603−4611.
10. Hooper, A. B., Debey, P., Andersson, K. K., and Balny, C. (1983) Heme-P460 of hydroxylamine oxidoreductase of *Nitrosomonas*—Reaction with CO and H_2O_2, *Eur. J. Biochem. 134*, 83−87.
11. Hooper, A. B., and Terry, K. R. (1977) Hydroxylamine oxidoreductase from *Nitrosomonas*—Inactivation by hydrogen peroxide, *Biochemistry 16*, 455−459.
12. Lipscomb, J. D., Andersson, K. K., Munck, E., Kent, T. A., and Hooper, A. B. (1982) Resolution of multiple heme centers of hydroxylamine oxidoreductase from *Nitrosomonas*. 2. Mössbauer spectroscopy, *Biochemistry 21*, 3973−3976.
13. Kowalchuk, G. A., and Stephen, J. R. (2001) Ammonia-oxidizing bacteria: A model for molecular microbial ecology, *Annu. Rev. Microbiol. 55*, 485−529.
14. Arciero, D. M., and Hooper, A. B. (1993) Hydroxylamine oxidoreductase from *Nitrosomonas europaea* is a multimer of an octa-heme subunit, *J. Biol. Chem. 268*, 14645−14654.
15. Igarashi, N., Moriyama, H., Fujiwara, T., Fukumori, Y., and Tanaka, N. (1997) The 2.8 Å structure of hydroxylamine oxidoreductase from a nitrifying chemoautotrophic bacterium, *Nitrosomonas europaea*, *Nat. Struct. Biol. 4*, 276−284.
16. Bergmann, D. J., and Hooper, A. B. (1994) The primary structure of cytochrome P460 of *Nitrosomonas europaea*—Presence of a *c*-heme binding motif, *FEBS Lett. 353*, 324−326.
17. Numata, M., Saito, T., Yamazaki, T., Fukumori, Y., and Yamanaka, T. (1990) Cytochrome P460 of *Nitrosomonas europaea*—Further purification and further characterization, *J. Biochem. 108*, 1016−1021.
18. Andersson, K. K., Babcock, G. T., and Hooper, A. B. (1991) P460 of Hydroxylamine oxidoreductase of *Nitrosomonas europaea*—Soret resonance Raman evidence for a novel heme-like structure, *Biochem. Biophys. Res. Commun. 174*, 358−363.
19. Miller, D. J., Wood, P. M., and Nicholas, D. J. D. (1984) Further characterization of cytochrome P460 in *Nitrosomonas europaea*, *J. Gen. Microbiol. 130*, 3049−3054.
20. Bergmann, D. J., Zahn, J. A., and DiSpirito, A. A. (2000) Primary structure of cytochrome *c*′ of *Methylococcus capsulatus* Bath: Evidence of a phylogenetic link between P460 and *c*′-type cytochromes, *Arch. Microbiol. 173*, 29−34.
21. Elmore, B. O., Bergmann, D. J., Klotz, M. G., and Hooper, A. B. (2007) Cytochromes P460 and *c*′-beta; a new family of high-spin cytochromes *c*, *FEBS Lett. 581*, 911−916.
22. Arciero, D. M., and Hooper, A. B. (1998) Consideration of a phlorin structure for haem P460 of hydroxylamine oxidoreductase and its implications regarding reaction mechanism, *Biochem. Soc. Trans. 26*, 385−389.
23. Arciero, D. M., and Hooper, A. B. (1997) Evidence for a crosslink between *c*-heme and a lysine residue in cytochrome P460 of *Nitrosomonas europaea*, *FEBS Lett. 410*, 457−460.

24. Bergmann, D. J., and Hooper, A. B. (2003) Cytochrome P460 of *Nitrosomonas europaea*—Formation of the heme-lysine cross-link in a heterologous host and mutagenic conversion to a non-cross-linked cytochrome *c*′, *Eur. J. Biochem. 270*, 1935−1941.
25. Elmore, B. O., Pearson, A. R., Wilmot, C. M., and Hooper, A. B. (2006) Expression, purification, crystallization and preliminary X-ray diffraction of a novel *Nitrosomonas europaea* cytochrome, cytochrome P460, *Acta Crystallogr., Sect. F: Struct. Biol. Cryst. Commun. 62*, 395−398.
26. Yang, C., Pflugrath, J. W., Courville, D. A., Stence, C. N., and Ferrara, J. D. (2003) Away from the edge: SAD phasing from the sulfur anomalous signal measured in-house with chromium radiation, *Acta Crystallogr., Sect. D: Biol. Crystallogr. 59*, 1943−1957.
27. Otwinowski, Z., and Minor, W. (1997) Processing of X-ray diffraction data collected in oscillation mode, *Methods Enzymol. 276*, 307−326.
28. CCP4 (1994) The CCP4 suite: Programmes for protein crystallography, *Acta Crystallogr., Sect. D: Biol. Crystallogr. 50*, 760−763.
29. Schneider, T. R., and Sheldrick, G. M. (2002) Substructure solution with SHELXD, *Acta Crystallogr., Sect. D: Biol. Crystallogr. 58*, 1772−1779.
30. de La Fortelle, E., and Bricogne, G. (1997) Maxiumum-likelihood heavy-atom parameter refinement in the MIR and MAD methods, *Methods Enzymol. 276*, 472−494.
31. Abrahams, J. P., and Leslie, A. G. (1996) Methods used in the structure determination of bovine mitochondrial F1 ATPase, *Acta Crystallogr., Sect. D: Biol. Crystallogr. 52*, 30−42.
32. Cowtan, K. (1994) "DM": An automated procedure for phase improvement by density modification, *Jt. CCP4 ESF-EACBM Newsl. Protein Crystallogr. 31*, 34−38.
33. Emsley, P., and Cowtan, K. (2004) Coot: Model-building tools for molecular graphics, *Acta Crystallogr., Sect. D: Biol. Crystallogr. 60*, 2126−2132.
34. Murshudov, G., Vagin, A., and Dodson, E. (1996) Application of maximum likelihood refinement, *Proceedings of Daresbury Study Weekend*, 93−104.
35. Murshudov, G. N., Lebedev, A., Vagin, A. A., Wilson, K. S., and Dodson, E. J. (1999) Efficient anisotropic refinement of macromolecular structures using FFT, *Acta Crystallogr., Sect. D: Biol. Crystallogr. 55*, 247−255.
36. Murshudov, G. N., Vagin, A. A., and Dodson, E. J. (1997) Refinement of macromolecular structures by the maximum-likelihood method, *Acta Crystallogr., Sect. D: Biol. Crystallogr. 53*, 240−255.
37. Laskowski, R. A., MacArthur, M. W., Moss, D. S., and Thornton, J. M. (1993) PROCHECK: A program to check the stereochemical quality of protein structures, *J. Appl. Crystallogr. 26*, 283−291.
38. Vaguine, A. A., Richelle, J., and Wodak, S. J. (1999) SFCHECK: A unified set of procedures for evaluating the quality of macromolecular structure-factor data and their agreement with atomic model, *Acta Crystallogr., Sect. D: Biol. Crystallogr. 55*, 191−205.
39. Pflugrath, J. W. (1999) The finer things in X-ray diffraction data collection, *Acta Crystallogr., Sect. D: Biol. Crystallogr. 55*, 1718−1725.
40. Volbeda, A. (1999) Speleologie des hydrogenases a nickel et a fer, *Les Ecoles Physique et Chimie du Vivant 1*, 47−52.
41. Dundas, J., Ouyang, Z., Tseng, J., Binkowski, A., Turpaz, Y., and Liang, J. (2006) CASTp: Computed atlas of surface topography of proteins with structural and topographical mapping of functionally annotated residues, *Nucleic Acids Res. 34*, W116−W118.
42. Delano, W. L. (2002) *The PyMOL Molecular Graphics System*, Delano Scientific, San Carlos, CA.
43. Petřek, M., Otyepka, M., Banáš, P., Košinová, P., Koča, J., and Damborsky, J. (2006) CAVER: A new tool to explore routes from protein clefts, pockets and cavities, *BMC Bioinformatics 7*, 316.
44. Jentzen, W., Ma, J. G., and Shelnutt, J. A. (1998) Conservation of the conformation of the porphyrin macrocycle in hemoproteins, *Biophys. J. 74*, 753−763.
45. Jentzen, W., Song, X. Z., and Shelnutt, J. A. (1997) Structural characterization of synthetic and protein-bound porphyrins in terms of the lowest-frequency normal coordinates of the macrocycle, *J. Phys. Chem. B 101*, 1684−1699.
46. Katoh, K., Kuma, K., Toh, H., and Miyata, T. (2005) MAFFT version 5: Improvement in accuracy of multiple sequence alignment, *Nucleic Acids Res. 33*, 511−518.
47. Katoh, K., Misawa, K., Kuma, K., and Miyata, T. (2002) MAFFT: A novel method for rapid multiple sequence alignment based on fast Fourier transform, *Nucleic Acids Res. 30*, 3059−3066.
48. Kleywegt, G. J., and Jones, T. A. (1998) Databases in protein crystallography, *Acta Crystallogr., Sect. D: Biol. Crystallogr. 54*, 1119−1131.
49. Holm, L., and Sander, C. (1996) Mapping the protein universe, *Science 273*, 595−603.
50. Molinspiration, Property Calculation Service.
51. Bollinger, J. A., Brown, D. E., and Dooley, D. M. (2005) The formation of lysine tyrosylquinone (LTQ) is a self-processing reaction. Expression and characterization of a *Drosophila* lysyl oxidase, *Biochemistry 44*, 11708−11714.
52. Colas, C., and de Montellano, P. R. O. (2003) Autocatalytic radical reactions in physiological prosthetic heme modification, *Chem. Rev. 103*, 2305−2332.
53. Zahn, J. A., Arciero, D. M., Hooper, A. B., and DiSpirito, A. A. (1996) Cytochrome *c*′ of *Methylococcus capsulatus* Bath, *Eur. J. Biochem. 240*, 684−691.
54. Lawson, D. M., Stevenson, C. E., Andrew, C. R., and Eady, R. R. (2000) Unprecedented proximal binding of nitric oxide to heme: Implications for guanylate cyclase, *EMBO J. 19*, 5661−5671.
55. Lawson, D. M., Stevenson, C. E., Andrew, C. R., George, S. J., and Eady, R. R. (2003) A two-faced molecule offers NO explanation: The proximal binding of nitric oxide to haem, *Biochem. Soc. Trans. 31*, 553−557.
56. Moir, J. W. (1999) Cytochrome *c*′ from *Paracoccus denitrificans*: Spectroscopic studies consistent with a role for the protein in nitric oxide metabolism, *Biochim. Biophys. Acta 1430*, 65−72.
57. Kruglik, S. G., Lambry, J. C., Cianetti, S., Martin, J. L., Eady, R. R., Andrew, C. R., and Negrerie, M. (2007) Molecular basis for nitric oxide dynamics and affinity with *Alcaligenes xylosoxidans* cytochrome *c*, *J. Biol. Chem. 282*, 5053−5062.
58. Harrison, F. (2007) Microbial ecology of the cystic fibrosis lung, *Microbiology 153*, 917−923.
59. Gasteiger, E., Hoogland, C., Gatticker, A., Duvaud, S., Wilkins, M. R., Appel, R. D., and Bairoch, A. (2005) Protein identification and analysis tools on the ExPASy server, in *The Proteomics Protocols Handbook* (Walker, J. M., Ed.), pp 571−607, Humana Press, Totowa, NJ.
60. Bond, C. S. (2003) TopDraw: A sketchpad for protein structure topology cartoons, *Bioinformatics 19*, 311−312.

BI700086R